Exploiting the Potential of Hybrid FMT/XCT Imaging by Means of Segmentation

Marcus Freyer, Angelique Ale, Ralf B. Schulz, Vasilis Ntziachristos, and Karl-Hans Englmeier
Chair for Biological Imaging, Technical University Munich, and Helmholtz Zentrum München, German Research Center for Environmental Health, Institute of Biological and Medical Imaging, Ingolstödter Landstraße 1, 85764 Neuherberg, Germany.
Author e-mail address: marcus.freyer@helmholtz-muenchen.de

Abstract: Hybrid FMT/XCT systems enable us to improve optical tomography image quality by using image priors in the reconstruction algorithm. We propose segmentation techniques to extract those priors and demonstrate their utilization in FMT image reconstruction.

1. Introduction

Optical tomography offers operational simplicity and rich contrast, especially when targeted fluorochromes are used. In particular fluorescence molecular tomography (FMT) is able to highly resolve cellular and sub-cellular contrast in whole animals [1]. In recent years, significant technological developments have exploited the potential of FMT further. Many scientists proposed the use of image priors to construct a more accurate solution to the forward problem or to regularize the ill-posed inverse problem [2]. This idea led to the development of hybrid imaging systems.

We developed a fully integrated FMT-XCT scanner that provides accurately registered data [3]. To yield the capability of the hybrid system, image priors have to be extracted from the CT images. Thus we consider herein an automatic segmentation framework to identify different organs and structures i.e. bones, lung and heart. The framework utilizes different image processing approaches to resolve the unique problems that emerge due to the differences between the respective structures.

2. Segmentation Framework

We consider the segmentation of three major structures in the mouse torso: bone, lung and heart. The selection results from the particular interest to study lung cancer and lung inflammatory diseases. The various segmentation approaches are described in the following.

2.1. Bone segmentation

Bone structures exhibit high contrast and intensities in CT images and thus can be easily identified using threshold approaches. The problem is rather the automatic detection of a correct threshold. Usually there is no standardized CT intensity scale in small animal imaging data acquisition like the Hounsfield scale in clinical data. Thus an appropriate threshold had to be found by analyzing the data.

We used an intensity histogram to detect certain features i.e. local maxima that mark certain tissues (soft tissue) and substances (air and water). Since skeletal tissue itself exhibits no distinct features in such a histogram itself, the maxima were used to approximate the threshold thereby assuming a constant relationship between different tissues/substances. Thus we could compute a feasible threshold in CT data with arbitrary units.

2.2. Lung segmentation

The lung segmentation was preceded by a ribcage detection step. This was necessary due to the fact that µCT images of mice possess a high amount of moving artefacts resulting in diffuse images. Thus the region of interest had to be confined as tight as possible around the structures we wished to detect to eliminate false segmentations. We used a Gabor filter to recognize the harmonic oscillations the ribcage produces in a histogram of the bone ratio per axial slice. We computed this histogram using the previously gained bone segmentation result. Thus we were able to approximate the beginning and end of the ribcage in axial direction accurate enough for our needs. The ribcage was also confined in the other directions by simply finding the first and last occurrences of bone voxels in the accordant histograms.

The lung itself was segmented using a standard region growing algorithm. The seed points for the procedure were automatically recognized by analyzing the histogram of CT intensities within the detected ribcage region. Like

for the previous detection of a threshold for the bone segmentation we searched for specific features in the histogram that allowed the approximation of the lung intensity thus providing voxels that served as seed point candidates. Finally only a small number of seed points were chosen randomly to limit time complexity.

2.3. Heart segmentation

The heart was segmented using a static model of a heart, generated from manually segmented training data. The model was initialized at a specified position inside the ribcage using again the ribcage detection for orientation. This approximation usually also created regions where segmentations were overlapping each other. Thus an iterative approach was used to push the heart model away from these regions onto the correct position.

For that purpose every overlapping voxel was used to generate a respective vector from each of those voxels to the centre of the heart. The resulting vector field was used to translate the heart to a more suitable position. This was repeated until no more overlapping regions could be found or the different vectors negated each other. The latter case implied that the model was too big to fit. If so, the heart model was shrunken und the iterative process was re-initialized.

3. FMT Reconstruction

For FMT we modelled photon propagation in the tissue by using the diffusion approximation to the radiative transport equation. For a solution to this equation we used Green's functions to model the spatially varying diffusion and absorption coefficients. Furthermore, to eliminate the influence of varying source intensities and detector sensitivities and to correct for heterogeneous optical coefficients, we used the normalized ratio between fluorescence and transmittance as presented in [4].

Through discretization, this equation can be transformed into the linear system $Wx=y$. Here W contains the contribution of the integral over the Green's functions, x is the discrete vector of the fluorochrome concentrations and y is the measurement vector. Since this equation is usually ill-conditioned a stable solution can be found by minimizing a regularized residual

$$\|Wx - y\|^2 + \lambda \|Lx\|^2 \to \min \qquad (1)$$

We integrated the anatomical priors from the segmentation results by using Laplace regularization [2]. Here L is defined by

$$L = \begin{bmatrix} l_{1,1} & l_{2,1} & \cdots & l_{w,1} \\ l_{1,2} & l_{2,2} & \ddots & \vdots \\ \vdots & \ddots & \ddots & l_{w,w-1} \\ l_{1,w} & \cdots & l_{w-1,w} & l_{w,w} \end{bmatrix} \qquad (2)$$

where w is the number of voxels in the CT date volume and l is thus given by

$$l_{i,j} = \begin{cases} 1 & \text{if } i = j \\ -\dfrac{1}{w_s} & \text{if voxels } i, j \text{ are part of the same region s} \\ 0 & \text{otherwise} \end{cases} \qquad (3)$$

with w_s being the number of voxels in region s. The regions are defined by the segmentations. The Laplace regularization smoothes the estimated fluorochrome distributions within a region while it allows strong differences across region boundaries. For comparison we also used the well known Thikonov regularization with $L=Id$ being the identity matrix. Thus, this regularization does not use anatomical priors.

4. Results

4.1. Segmentation Framework

The results of our segmentation framework are illustrated in Fig. 1. The whole segmentation procedure of a volume with approximately 30 million voxels takes about 2 minutes. To measure the segmentation quality we used the Dice coefficient, the false acceptance and false rejection rate. The bone segmentation had the best quality, reaching a Dice coefficient of approximately 0.87. Lung and heart segmentation reached about 0.76. This was influenced mostly due to a high false rejection rates (in both cases over 0.31). For lung segmentation this was usually the result of pathologies that led to regions of unusual intensities within the lung. The heart segmentation suffers from the solid model that could not perfectly adapt to the form variability of the organ.

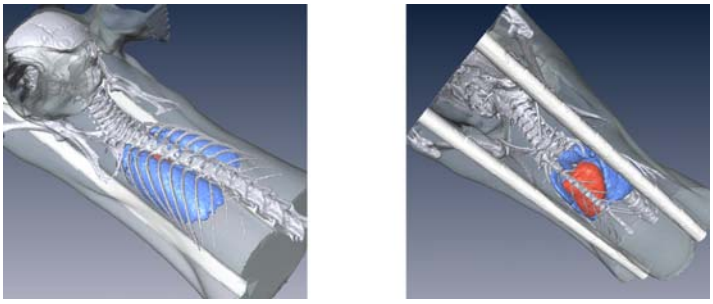

Fig. 1: Result of the segmentation framework. Mouse skeleton (grey), lung (blue) and heart (red) inside the transparent body of the mouse, lying on a specimen holder (white). Body and specimen holder were segmented using a simple thresholding algorithm. The specimen holder was later separated manually for visualization purposes.

4.2. FMT Reconstruction

We could see significant improvements in FMT reconstruction on simulated data, modelled after previous studies of lung inflammation. Without any regularization, the reconstruction failed, producing significant artefacts especially along tissue borders. The Thikonov regularization could remove those artefacts but the images where still heavily blurred and the reconstructed fluorochrome concentration was to low. Only the Laplace regularization using anatomical priors showed satisfying results. The intensity was reconstructed correctly and the images where only slightly blurred along the borders.

5. Discussion

We introduced a fast automatic framework for the segmentation of multiple anatomical structures in CT images and showed its utilization for improving FMT image reconstruction. The results have shown that the framework still suffers from a high false rejection rate. Most notably the solid model of the heart restrains the segmentation quality. Here deformable models could improve the results but they are certainly more time consuming than this approach. Nevertheless, the segmentation results were appropriate enough to improve FMT image quality significantly. Thus it remains open, if more accurate but time consuming segmentation methods would be a benefit for this kind of application. We think that the focus for further studies should be on the segmentation of more anatomical structures rather than on achieving higher quality segmentation results.

References

[1] V. Ntziachristos, J. Ripoll, L.H.V. Wang, R. Weissleder, “Looking and listening to light: the evolution of whole-body photonic imaging”, Nat. Biotechnol. 23(3), 313-320 (2005).

[2] S.C. Davis, H. Dehghani, J. Wang, S. Jiang, B.W. Pogue, K.D. Paulsen, „Image-guided diffuse optical fluorescence tomography implemented with Laplacian-type regularization”, Opt Express 15(7), 4066-4082 (2007).

[3] R.B. Schulz, A. Ale, A. Sarantopoulos, M. Freyer, E. Soehngen, M. Zientkowska, V. Ntziachristos, „Hybrid System for Simultaneous Fluorescence and X-ray Computed Tomography”, IEEE Trans. Med. Imaging [Epub ahead of print], PMID: 19906585 [PubMed - as supplied by publisher] (2009).

[4] V. Ntziachristos, R. Weissleder, „Experimental three-dimensional fluorescence reconstruction of diffuse media by use of a normalized Born approximation”, Opt. Lett. 26(12), 893-895 (2001).